Finite Elements in Analysis and Design 134 (2017) 16–26

Contents lists available at ScienceDirect

Finite Elements in Analysis and Design

journal homepage: www.elsevier.com/locate/finel

Implementation of topological derivative in the moving morphable components approach

Meisam Takalloozadeh, Gil Ho Yoon*

School of Mechanical Engineering, Hanyang University, Seoul, Republic of Korea

ARTICLE INFO

Keywords:
Topology optimization
Moving morphable components
Topological derivative
Stress-based optimization
Thermal loading

ABSTRACT

We propose a new topology optimization approach based on the moving morphable components (MMC) framework with an explicitly described a layout through a finite number of components. The position and shape values of each component were defined as design variables. In this study, a method was developed by utilizing topological derivative. Instead of performing a discrete sensitivity analysis based on finite element methods, a topological derivative was used to calculate the first derivative of an objective function with respect to the shape and position of the components. The obtained derivative was validated via discrete sensitivity analysis. The topological derivative formulation has been well developed in recent years for different structural and non-structural problems. Utilizing this powerful tool enabled the MMC approach to easily solve various types of topology optimization problems. Herein, the presented method is illustrated through several topology optimization problems such as stress-based and thermo-mechanical topology optimization.

1. Introduction

The objective of this work is to develop a moving morphable components (MMC) framework approach based on the topological derivative concept. The MMC approach utilized a finite number of movable and deformable components to define the layout of a structure. By moving or changing the shape of these components during the optimization process, some empty spaces were either created in the design domain or were filled with materials (Fig. 1). On the other hand, a topological derivative is defined as the effect of an infinitesimal change in topology with regard to the quantity of an objective function. This topological change could be the insertion of a small hole in the domain or the addition of a small amount of material to the structure layout. Therefore, the concept of a topological derivative could be utilized in the MMC approach if we were to calculate the topological derivative during changes in position or shape of the components.

1.1. Topology optimization methods

Topology optimization (TO) is one of the most popular methods used for structural optimization, having rapidly extended from academic research to industrial applications [1]. The TO method fundamentally optimizes the geometry over arbitrary domains. This method was introduced via the Homogenization approach [2], in which varying material properties in space are described by composite materials. Later, TO was developed via two popular strategies, the solid isotropic material with penalization (SIMP) method [3] and topology optimization based on the level-set method [4–6]. There are also new alternative approaches with regard to TO [7,8].

In the SIMP method, the values of pseudo-densities assigned to elements were found to minimize the objective function [9]. The objective function in the majority of structural optimization studies was compliance [10], but other practical cost functions such as stress, displacement, and natural frequency were considered by the SIMP method. The SIMP method was relatively easy to implement [11] and well-developed, being utilized to solve structural and non-structural multi-physics systems [12–16].

As the SIMP method uses the pseudo-density in each element of the finite element method, the obtained layout possessed jagged shapes at the boundaries. By contrast, in the level-set based method, the design domain was specified by a surface defined by a level-set function; therefore, smooth boundaries could be obtained [5,17,18]. Indeed, the interface between material phases was defined implicitly by iso-contours of the scalar level-set function at all times, so the domain was well defined and singularity problems did not arise [19]. There were also many formulations and implementations of the level-set based method [20].

Several common problems in engineering have been considered in the TO. For example, one important problem involved a consideration

* Corresponding author.
E-mail addresses: ghy@hanyang.ac.kr, gilho.yoon@gmail.com (G.H. Yoon).

http://dx.doi.org/10.1016/j.finel.2017.05.008
Received 3 February 2017; Received in revised form 18 April 2017; Accepted 15 May 2017
Available online 03 June 2017
0168-874X/

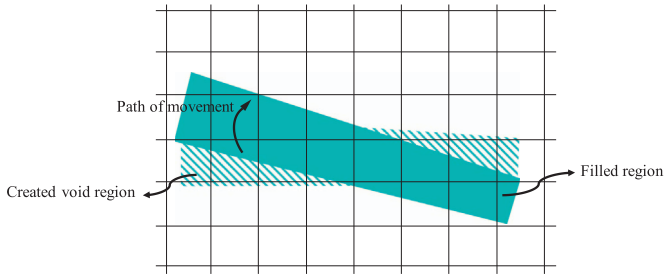

Fig. 1. Movement of a component in the design domain and background mesh.

of stress constraints in the design process [10]. SIMP and level-set based methods were well investigated with regard to solving stress constrained TO problems [21–23]. After the earliest work by Yang and Chen [24], several problems were addressed in the stress constrained TO. These issues could be categorized as singularity issues, highly nonlinear behaviors, and the local behavior of stress constraints [25]. Several methods such as epsilon-relaxation [26], qp-relaxation [27], relaxed stress indicators [28], Kreisselmeier–Steinhauser functions [29], and p-norms [27,30] were utilized to overcome the aforementioned problems.

Another common type of engineering problem considered in TO is thermo-mechanical problems. The earliest works in this field date back to 1995 [31]. The authors of [31] addressed the strong dependency of optimum design on temperature differentials. Xia and Wang [32] used the level-set based method to consider thermal effects with regard to structural optimization. In their study, the mean compliance was minimized and a geometric energy term was introduced to obtain a smooth boundary. Despite an easy implementation of the SIMP method in thermo-mechanical problems, zero density in elements required careful treatment such as the epsilon-method [26] due to singularity issues. Deaton et al. [33] demonstrated that typical compliance minimization in thermo-elastic problems may not generate favorable design, the reason being due to the design-dependency of the thermal load, which was subject to thermo-elastic effects during topology optimization. Moreover, compliant mechanism problems were solved by considering thermal effects in [34].

In both the SIMP and the level-set based method, an implicit definition of the boundary was obtained, which yielded some difficulties. For example, it is important to possess shape feature control during manufacturing [35,36], which is difficult in implicit ways due to special techniques that are necessary for length scale control. Moreover, the structural geometry needed in computer-aided design (CAD) is different from what is represented by implicit ways. This made it difficult to establish a link between CAD and the obtained layout during the optimization process [37]. Another drawback of implicitly defining the layout is the large number of required design variables, especially in 3D problems. By contrast to common methods in TO such as the SIMP and the level-set based methods, there is a new approach referred to as the moving morphable components (MMC) method, in which boundaries are explicitly defined by a polynomial function [8]. This method is described in the following sections and in Section 2.1.

1.2. MMC approach

A novel and practical approach in TO, referred to as the moving morphable components method, utilizes morphable components that can move and reshape to find the optimum layout of a structure under the given boundary conditions [8,38–41]. Indeed, this approach could be a bridge between size, shape, and topology optimization. The shapes of components were defined by an explicit boundary, which were functions of a finite number of variables [8]. These variables for all components in addition to the positions of the components were design variables during the optimization process. For example, one could use some bars with a constant thickness as components to define a 2D layout within the design domain (D). This design domain is presented as a dashed line in Fig. 2. In this example, the layout was explicitly defined by four bars and the number of design variables for each component was five: the x and y coordinates of the bar center and the length (L), thickness (t), and angle of the bar with a horizontal axis (θ). The total number of design variables for this example was $4 \times 5 = 20$. This requirement to lower the number of design variables defining a layout was another advantage of the MMC approach. Obviously, one could use components with different shapes and design variables, but the boundary of the layout was still explicitly defined. Additional parameters to define the shapes of components led to more flexible shapes for the components, but would increase computational costs.

1.3. Sensitivity analysis and topological derivative

Design sensitivity analysis is a crucial issue in the field of topology optimization. This analysis is used to compute the rate of change of a cost function, such as a change in strain energy or stress, with respect to changes in the design variables. Sensitivity analysis guided the optimization algorithms (i.e., SLP, MMA) to redistribute material within the design domain to determine the optimum layout. There are three approaches in the design sensitivity analysis: the approximation, discrete, and continuum approaches [42]. The approximation approach utilized finite difference methods to calculate design sensitivity. In the discrete approach, discrete FEM governing equations are used to obtain derivatives. In this approach, taking the derivative of the stiffness matrix is always necessary. This approach is widely used during topology optimization, particularly in the SIMP method. The continuum approach in design sensitivity analysis took the design derivative of the variational equation before it was discretized. One of the most powerful methods in this approach is the topological derivative.

The topological derivative concept was proposed in [43] and was later developed in several studies [44,45]. It possessed several applications with regard to shape and topology optimization, image processing, and mechanical modeling [46]. This concept expressed changes in

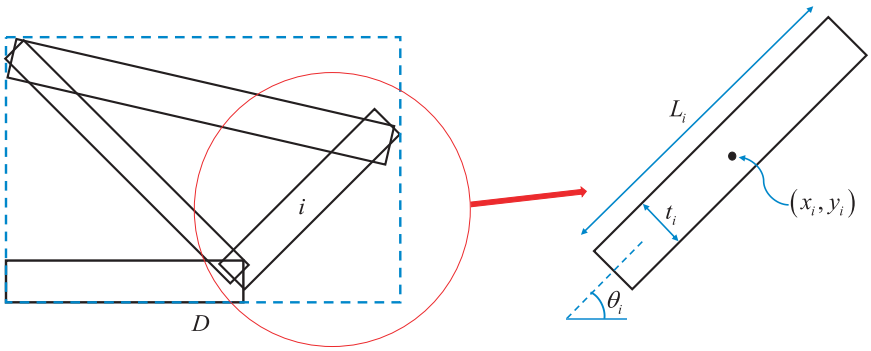

Fig. 2. Defining the layout of a structure with bars.

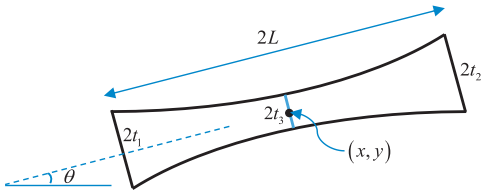

Fig. 3. Component shape and design variables.

the objective function with respect to infinitesimal changes in topology. Topological changes are defined by adding or removing material to the structural domain. There are two major methods to obtain a topological derivative: (i) asymptotic expansion of an objective functional [47] and (ii) the shape derivative of a very small hole [48]. Topological derivative concepts were previously used in the level-set based method to obtain the optimum topology [6]. In that approach, topological derivatives were utilized as a guide to introduce holes into an auxiliary level-set. By using this concept, the optimal layout was independent of the number of holes in the initial domain [20]. Another approach directly used the topological derivative as a level-set [49,50]. The optimum topology in this approach was extracted by using a cutting-plane on the topological sensitivity field.

In the present study, a new alternative approach using topological derivatives in TO was proposed. A novel MMC method was developed by utilizing a topological derivative. The topological derivative formulation has been fully developed for lots of common problems in structural and non-structural problems. These problems include any relevant physics and engineering problems modeled by partial differential equations. For instance, the derivative formulation for the stress constrained of ductile material was proposed in [22,51] and for brittle materials by Amstutz et al. [52]. The compliant mechanism problem is solved by topological derivative [53,54]. The derivative for the steady-state heat diffusion problems is obtained in [55]. Moreover, multi load case and multi constrained formulation are derived in [19,56]. Topological derivative is applied to find the optimum configuration for the antenna [57] and it is also used in optimum designing of inductors in electromagnetic casting [58]. Thermo-mechanical formulation is presented in [59,60]. Topological derivative of the total potential energy of an elastic cracked body is calculated in [61,62]. Fluid flow channel is designed by applying topological derivative [63]. Topological derivative for acoustic problems is used in sound scattering problems [64]. The reader can find more formulations in [46]. Developing MMC approach by topological sensitivity concept enables this approach to solve the mentioned problems easily.

Details and calculations of the topological derivative in the MMC approach are provided in the next section. The results of both sensitivity analyses, using finite elements and the topological derivative, were compared for compliance minimization problems. Section 3 introduces the topological derivative for several popular types of TO problems and several examples are provided to show the ability and efficiency of the MMC approach based on topological derivatives. Finally, Section 4 concludes this study.

2. Discrete and continuum sensitivity analysis

2.1. Formulation of the MMC framework approach

In the MMC framework approach, structure topology is described by the topology description function (TDF, ϕ), as follows [8]:

$$\begin{cases} \phi(\mathbf{x}) > 0 & \text{if } \mathbf{x} \in \Omega \\ \phi(\mathbf{x}) = 0 & \text{if } \mathbf{x} \in \partial\Omega \\ \phi(\mathbf{x}) < 0 & \text{if } \mathbf{x} \in D/\Omega \end{cases} \tag{1}$$

Here, Ω is a topology that must be computed within domain D and position vector is denoted by $\mathbf{x}$. If the number of components is N and $\phi_i = \phi_i(\mathbf{x})$ is the topology description function of the $i-th$ component, then:

$$\phi(\mathbf{x}) = \max(\phi_1, \ldots, \phi_i, \ldots, \phi_N) \tag{2}$$

The TDF of each component (ϕ_i) defines the region occupied by the following component:

$$\begin{cases} \phi_i(\mathbf{x}) > 0 & \text{if } \mathbf{x} \in \Omega_i \\ \phi_i(\mathbf{x}) = 0 & \text{if } \mathbf{x} \in \partial\Omega_i \\ \phi_i(\mathbf{x}) < 0 & \text{if } \mathbf{x} \in D/\Omega_i \end{cases} \tag{3}$$

For each component, the TDF can be described in different ways based on the shape of the component. More complex shapes possess additional design variables, leading to greater computation costs, but having more flexibility when defining layouts. With regard to 2D problems, one can use a bar with quadratic changes in thickness as a component (Fig. 3) [40]:

$$\begin{aligned} &\phi_i(x, y) = \left(\frac{x'}{L}\right)^m + \left(\frac{y'}{f(x')}\right)^m - 1 \\ &f(x') = \frac{t_1 + t_2 - 2t_3}{2L^2}x'^2 + \frac{t_2 - t_1}{2L}x' + t_3 \\ &\begin{Bmatrix} x' \\ y' \end{Bmatrix} = \begin{bmatrix} \cos\theta & \sin\theta \\ -\sin\theta & \cos\theta \end{bmatrix} \begin{Bmatrix} x \\ y \end{Bmatrix} \end{aligned} \tag{4}$$

Here, t_1, t_2, and t_3 are the component thickness values in three sections which are shown in Fig. 3; L is the length of the component. Angle θ is measured from the horizontal axis from the anti-clockwise direction. In the equation above, value m is a large even integer number to sharpen the edge of the component.

In general, two parameters (x, y) were used to determine the position of a component and five parameters explicitly described the shape of each component. The layout was made by all components; therefore, the boundary and geometry features of the final layout could be defined by an explicit description [40].

To analyze structures using the MMC approach, an Eulerian mesh was utilized and the TDF (ϕ) was calculated at each node. The Young's modulus (E^e) for the e-th element was then computed as follows [8]:

$$E^e = \frac{E_0\left(\sum_{j=1}^{4}(H(\phi_j^e))^q\right)}{4} \tag{5}$$

In the above equations, q is an integer number selected equal to 2, E_0 is the Young's modulus of the element material, and H is the smoothed Heaviside function:

$$H(x) = \begin{cases} 1 & \text{if } \varepsilon < x \\ \frac{3(1-\alpha)}{4} \times \left(\frac{x}{\varepsilon} - \frac{x^3}{3\varepsilon^3}\right) + \frac{1+\alpha}{2} & \text{if } -\varepsilon \le x \le \varepsilon \\ \alpha & \text{if } x < -\varepsilon \end{cases} \tag{6}$$

The shape of this function with two arbitrary values is depicted in Fig. 4. A small positive nonzero value ($\alpha = 0.001$) was selected to avoid

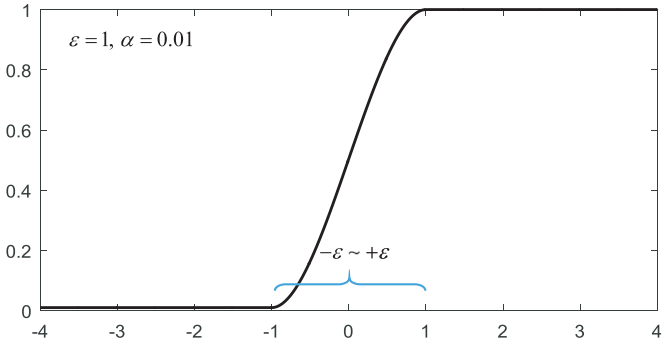

Fig. 4. Smoothed Heaviside function.

singularity of the global stiffness matrix and ε was set to four times the minimum side of the element. Indeed, $\alpha^q = 10^{-6} N/m^2$ defined the Young's modulus as a weak material to mimic voids in the design domain. After obtaining the Young's modulus for each element, the stiffness matrix of the e-th element ($\boldsymbol{k}^e$) was computed as follows:

$$\boldsymbol{k}^e = E^e \, \boldsymbol{k}^s \tag{7}$$

Here, $\boldsymbol{k}^s$ is the stiffness matrix of the elements regardless of component occupation. Obviously, if a uniform mesh was used, this matrix was the same for all elements.

2.2. Calculation and implementation of the topological derivative

A compliance (C) minimization problem using the MMC approach could be formulated as follows:

$$\begin{aligned} &\text{Find } \mathbf{DV} = \{\mathbf{DV}_1, \mathbf{DV}_2, \ldots, \mathbf{DV}_i, \ldots, \mathbf{DV}_N\} \\ &\underset{\Omega \subset D}{\text{Min}} \quad C = \mathbf{U}^{\mathrm{T}}\mathbf{F} \\ &\text{Subject to:} \\ &\quad |\Omega| = |\Omega|^* \\ &\quad \mathbf{KU} = \mathbf{F} \end{aligned} \tag{8}$$

The global stiffness matrix, nodal displacements, and global load vector were denoted by $\mathbf{K}$, $\mathbf{U}$, and $\mathbf{F}$, respectively. The final volume $|\Omega|^*$ is the only constraint during the optimization process. $\mathbf{DV}_i$ is the design variable vector of the i-th component, which defines the shape and position of the following component (Fig. 3):

$$\mathbf{DV}_i = \{x, y, L, t_1, t_2, t_3, \theta\}_i \tag{9}$$

Thus, the total number of design variables is $7 \times N$. To solve the above problem using MMC, the sensitivity of compliance with respect to each design variable (a) is required [40]. Utilizing the finite element method to analyze the structure, possessing the stiffness matrix ($\boldsymbol{K}$) and nodal displacement ($\boldsymbol{U}$) values, we could write the following:

$$C = \boldsymbol{U}^T \boldsymbol{K} \boldsymbol{U} \Rightarrow \frac{\partial C}{\partial a} = \frac{\partial \boldsymbol{U}^T}{\partial a} \boldsymbol{K} \boldsymbol{U} + \boldsymbol{U}^T \frac{\partial \boldsymbol{K}}{\partial a} \boldsymbol{U} + \boldsymbol{U}^T \boldsymbol{K} \frac{\partial \boldsymbol{U}}{\partial a} \tag{10}$$

On the other hand, from the equilibrium equation:

$$\boldsymbol{F} = \boldsymbol{K}\boldsymbol{U} \Rightarrow \frac{\partial \boldsymbol{F}}{\partial a} = \frac{\partial \boldsymbol{K}}{\partial a}\boldsymbol{U} + \boldsymbol{K}\frac{\partial \boldsymbol{U}}{\partial a} \Rightarrow \frac{\partial \boldsymbol{U}}{\partial a} = \boldsymbol{K}^{-1}\frac{\partial \boldsymbol{F}}{\partial a} - \boldsymbol{K}^{-1}\frac{\partial \boldsymbol{K}}{\partial a}\boldsymbol{U} \tag{11}$$

Thus, we could rewrite the derivative of compliance as follows:

$$\begin{aligned} &\frac{\partial C}{\partial a} = \left(\boldsymbol{K}^{-1}\frac{\partial \boldsymbol{F}}{\partial a} - \boldsymbol{K}^{-1}\frac{\partial \boldsymbol{K}}{\partial a}\boldsymbol{U}\right)^T \boldsymbol{K}\boldsymbol{U} + \boldsymbol{U}^T\frac{\partial \boldsymbol{K}}{\partial a}\boldsymbol{U} + \boldsymbol{U}^T\boldsymbol{K}\left(\boldsymbol{K}^{-1}\frac{\partial \boldsymbol{F}}{\partial a} - \boldsymbol{K}^{-1}\frac{\partial \boldsymbol{K}}{\partial a}\boldsymbol{U}\right) \\ &\Rightarrow \frac{\partial C}{\partial a} = 2\boldsymbol{U}^T\frac{\partial \boldsymbol{F}}{\partial a} - \boldsymbol{U}^T\frac{\partial \boldsymbol{K}}{\partial a}\boldsymbol{U} \end{aligned} \tag{12}$$

In the absence of the design dependent force, the above relation can be simplified:

$$\frac{\partial C}{\partial a} = -\boldsymbol{U}^T\frac{\partial \boldsymbol{K}}{\partial a}\boldsymbol{U} \tag{13}$$

By substituting Eqs. (5) and (7), the derivative of the stiffness matrix in Eq. (13) could be written as follows:

$$\frac{\partial \boldsymbol{K}}{\partial a} = \sum_{e=1}^{NE} \frac{\partial}{\partial a}\boldsymbol{k}^e = \frac{E}{4}\sum_{e=1}^{NE}\left(\sum_{i=1}^{4} q\left(H(\phi_i^e)\right)^{q-1}\frac{\partial}{\partial a}H(\phi_i^e)\right)\boldsymbol{k}^s \tag{14}$$

Here, NE is the number of elements. The above calculation was based on discretizing the domain to its finite elements, referred to as discrete structural sensitivity analysis. Another approach to calculate the sensitivity of compliance with respect to design variables involved utilizing the topological derivative. To introduce this concept, a structural domain was assumed with some small inserted holes (Fig. 5). The topological derivative, $D\psi$, for the objective function ψ could be defined as follows:

$$D\psi = \lim_{A \to 0} \frac{\psi(\Omega') - \psi(\Omega)}{A = \sum A_i} \tag{15}$$

Here, Ω and Ω' are domains prior to and after topological changes, respectively, and A_i is the area of the i-th small hole. If one were to consider the total strain energy as an objective function ($\psi = C$), for a 2D structure under a mechanical load, the topological derivative field (T) introduced in Eq. (15) could be obtained as follows [44,65]:

$$T = \frac{4}{1+\nu}\boldsymbol{\sigma}(\mathbf{u}) : \boldsymbol{\varepsilon}(\mathbf{u}) - \frac{1-3\nu}{1-\nu^2}\mathrm{tr}\boldsymbol{\sigma}(\mathbf{u})\mathrm{tr}\boldsymbol{\varepsilon}(\mathbf{u}) \tag{16}$$

Here, the Cauchy stress tensor, strain tensor, displacement field vector, and Poisson's ratio are denoted by $\boldsymbol{\sigma}(\mathbf{u})$, $\boldsymbol{\varepsilon}(\mathbf{u})$, $\mathbf{u}$, and ν, respectively. Stress and strain values were calculated at the point where a small hole was inserted.

By moving or changing the shape of the components, some void regions arose in the design domain and some void regions were filled with material as well. This state is presented schematically by moving a typical component in Fig. 6. Therefore, the derivative of compliance with respect to design variables ($\frac{\partial C}{\partial a}$) could be calculated via the topological derivative concept if the total topological derivative changes were calculated during changes in the design variables. For this purpose, one should calculate a summation of the topological changes due to component shape or positional changes:

$$\frac{\partial C}{\partial a} = \int_{\Omega} T dA \tag{17}$$

The above integration could be rewritten in the summation form as follows:

$$\frac{\partial C}{\partial a} = \sum_{e=1}^{NE} T^e dA^e \tag{18}$$

Having the TDF at all nodes, the area of the e-th element was calculated to be:

$$A^e = \frac{\sum_{i=1}^{4} H(\phi_i^e)}{4} A_s^e \tag{19}$$

Here, A_s^e is the area of the element regardless of component occupation. Moving or reshaping a component could yield a typical change in the TDF of each node as seen in Fig. 7. The filled part of the element depicted the parts of the element covered by a component. Obviously, the value of H for the structural domain nodes was one. By substituting Eq. (19) with Eq. (18), we finally yielded a change in compliance with respect to design variables:

$$\frac{\partial C}{\partial a} = \sum_{e=1}^{NE}\left(\sum_{i=1}^{4} T_i^e \times \frac{\partial}{\partial a}H(\phi_i^e) \times \frac{A_s^e}{4}\right) \tag{20}$$

Since $\phi(\mathbf{x})$ is an explicit function, the value of $\frac{\partial}{\partial a}H(\phi_i^e)$ could be calculated easily. Note that T_i^e is the function of stress and strain at the i-th node of the e-th element. By calculating the topological derivative at each node, the required sensitivity of compliance for the MMC approach could be achieved. It should be mentioned that as the Young's modulus was calculated from Eq. (5) by assuming $\mathbf{C}$ to be the elastic coefficient tensor, the stress at each element ($\boldsymbol{\sigma}^e$) could be obtained as follows:

$$\boldsymbol{\sigma}^e = \frac{\left(\sum_{i=1}^{4} (H(\phi_i^e))^q\right)}{4} \times \mathbf{C}\boldsymbol{\varepsilon}^e \tag{21}$$

Here, $\boldsymbol{\varepsilon}^e$ is the strain tensor for the e-th element.

2.3. Numerical validation

A rectangular design domain with clamped right and left edges was considered to be an example to compare the results from Eqs. (13) and (20) (Fig. 8). A downward unit point load was applied at the bottom

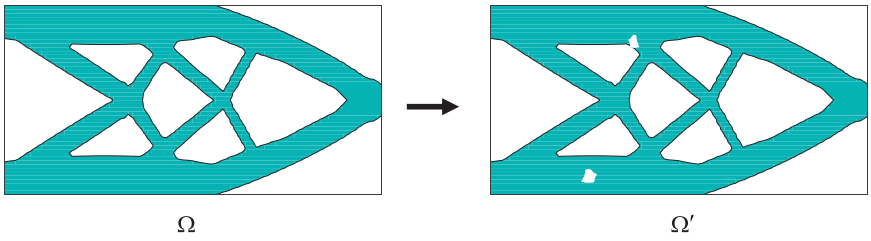

Fig. 5. Topological changes in the structural domain.

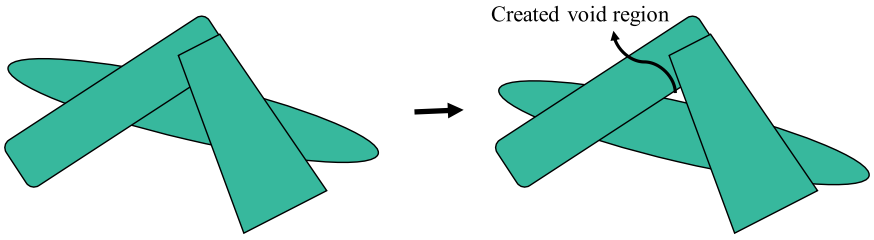

Fig. 6. Topological changes during the movement of a component.

center of the domain. The domain is discretized to 5000 elements and 16 components are used to define the layout; thus the total number of design variables are 112. The obtained derivatives are normalized by dividing all sensitivity values ($C_i = \partial C/\partial a_i$) to the maximum of absolute values: $\widetilde{C}_i = C_i/\max(|C_i|)$. The normalized derivative of compliance with respect to the design variables was computed once by Eq. (13) and once again by Eq. (20), the results of which can be seen in Fig. 9(a). Moreover, the difference between the two results can be seen in Fig. 9(b). The results of the two approaches were in fair agreement and the maximum absolute difference between the two was 0.049.

Moreover, Fig. 10 depicts the optimum layout for this example obtained via discrete compliance sensitivity using FEM (Fig. 10(a)) and the optimum topology obtained via topological derivative methods (Fig. 10(b)), in which the final mass was set to 40% of the initial mass. The history of compliance during optimization is shown in Fig. 10(c). As can be seen, the final layouts from both approaches were almost the same. It is worth mentioning that no filters were applied with regard to the topological derivative field. These results show the accuracy and efficiency of the obtained formula (Eq. (20)) and can be utilized in the MMC approach instead of calculating a discrete sensitivity analysis.

2.4. Calculating the TDF at the centers of elements

To compute the topological derivative at any point, the stress must be known at the point of interest (Eqs. (16 and 20)). In the finite element method, stress values were calculated at the Gaussian points (here, the centers of elements). On the other hand, to calculate sensitivity in the MMC approach, we needed to calculate the topological

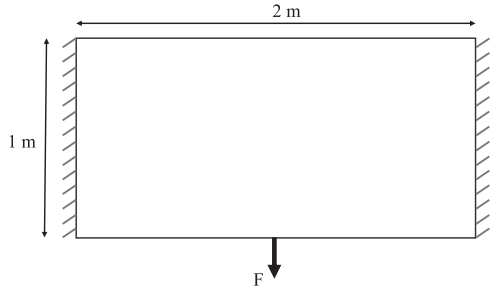

Fig. 8. The design domain and boundary conditions ($E = 1\text{N/m}^2$, $\nu = 0.33$ and $F = 1$ N).

derivative at each node (T_i^e). Thus, after obtaining the topological derivative at the centers of the elements, we could obtain the topological derivative at nodes via linear interpolation. Instead, one might be interested in calculating the TDF at the centers of elements to avoid this interpolation. In this case, the Young's modulus of each element was easily obtained as follows:

$$E^e = E_0(H(\phi^e))^q \tag{22}$$

Note that the TDF and Heaviside functions were calculated for each element as opposed to each node, and the derivative of compliance was obtained as follows:

$$\frac{\partial C}{\partial a} = \sum_{e=1}^{NE}\left(T^e \times \frac{\partial}{\partial a}H(\phi^e) \times A_s^e\right) \tag{23}$$

The optimal layout for the problem introduced in Fig. 8 was obtained by calculating the TDF at the centers of the elements

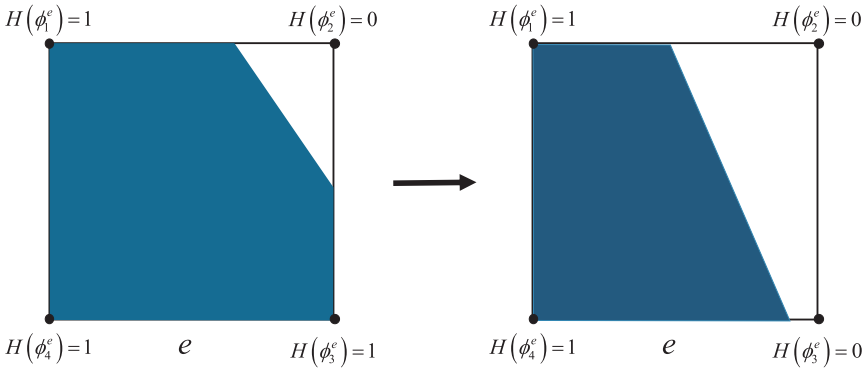

Fig. 7. Changes in the e-th element during component movement or reshaping.

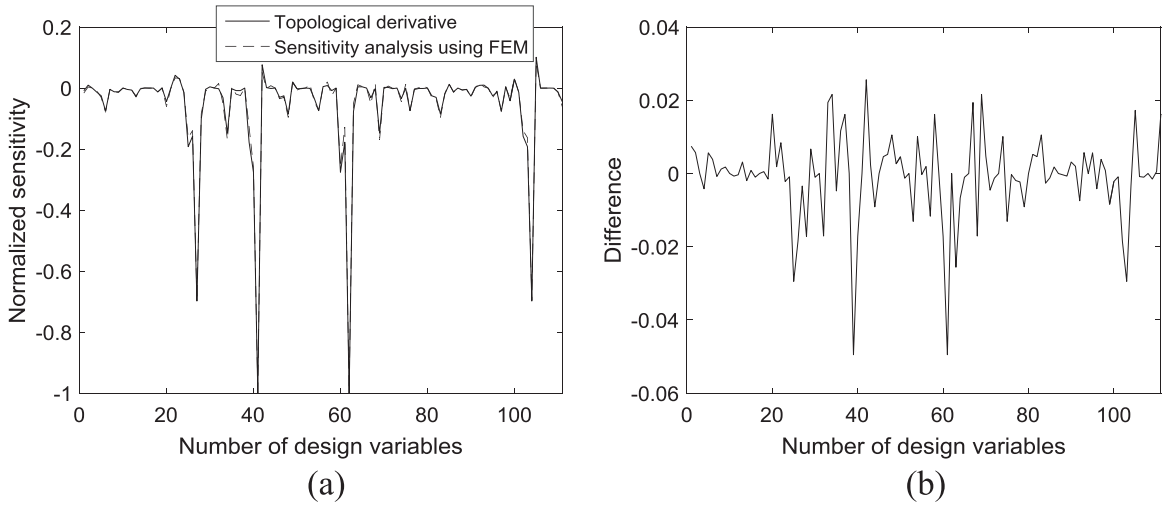

Fig. 9. (a) Sensitivity analysis results from discrete sensitivity analysis and topological derivative analysis, and (b) the difference between the topological sensitivity values and the discrete sensitivity.

(Fig. 11). As can be seen, the layout was almost the same as the result obtained in Fig. 10. Here, the computational cost was a little less but the final compliance was a little more.

For the rest of the examples, we calculated the topological derivative at nodes by using Eq. 20. Now, one could exploit this formula to solve other types of TO problems, a description of which is provided in the next section.

3. Numerical examples

In this section, several benchmark examples are provided to demonstrate the efficiency of the presented approach to solve common structural problems in TO. These examples contain thermo-mechanical and stress-based TO problems. Mathematical formulations and topological sensitivity formulas for each problem are also illustrated. Without loss of generality, the following material properties were chosen for the Young's modulus, Poisson ratio, and coefficient of thermal expansion: $E = 1\text{N/m}^2, \nu = 0.33$ and $\alpha_t = 1 \times 10^{-2}\text{K}^{-1}$. Before solving the benchmark examples, there is a discussion on the effects of component shape with regard to achieving optimum results.

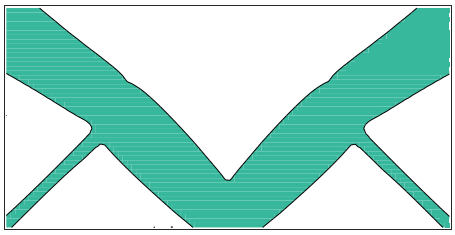

Fig. 11. Optimal layout by calculating the TDF at the centers of the elements ($C = 5.785$ J).

3.1. Effects of component shape

A bar with a quadratic change in thickness was utilized by Guo,

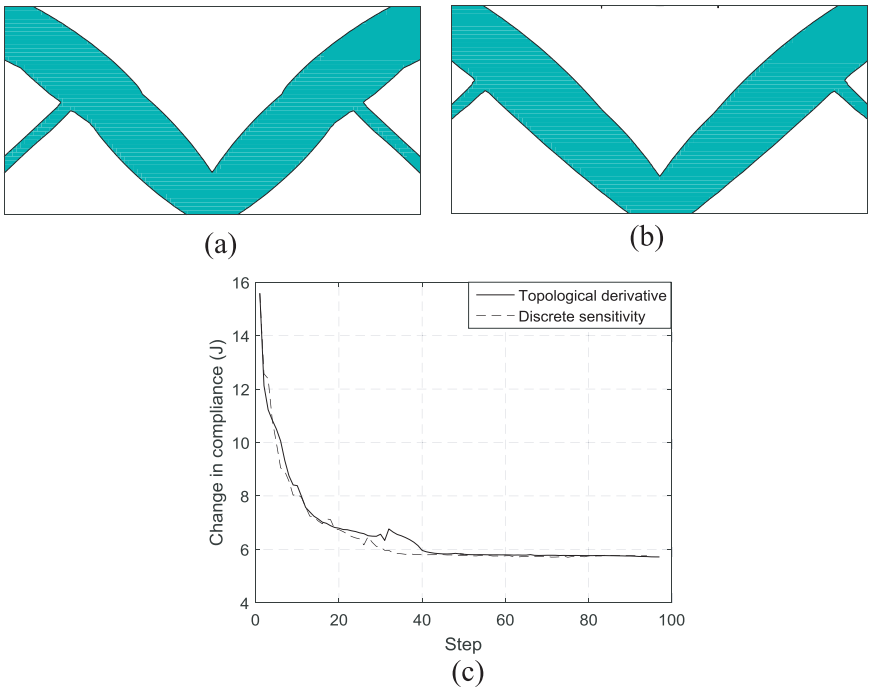

Fig. 10. Optimal layout ($|\Omega|^* = 0.4\,|\Omega|_{initial}$) using: (a) discrete sensitivity analysis ($C = 5.758$ J), (b) the topological derivative ($C = 5.738$ J) and (c) history of the objective function.

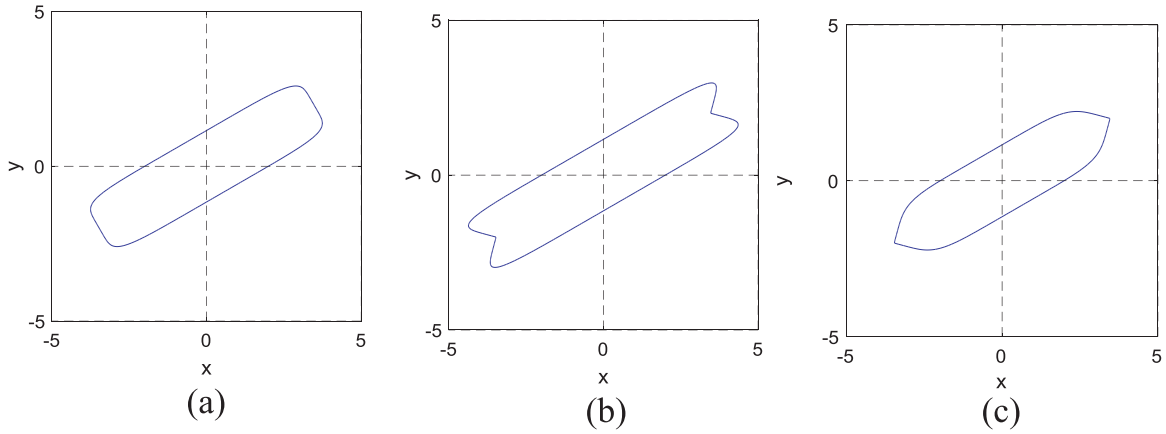

Fig. 12. Shapes of components: (a) ($g(y') = 4$), (b) ($g(y') = 4 + 1 \times |y'|$), and (c) ($g(y') = 4 - 1 \times |y'|$).

et al. [40] The shape of this bar for a uniform thickness case can be seen in Fig. 12(a). The value of m in Eq. (4) was selected to be 6. The shapes of the lines along the bar were second order polynomial, but at the start and end of the bar there were two straight lines perpendicular to the direction of the bar. A new design variable (η) was added to the TDF to change the shape of these parts (Eq. (24)).

$$\phi_i(x, y) = \left(\frac{x'}{g(y')}\right)^m + \left(\frac{y'}{f(x')}\right)^m - 1$$
$$g(y') = L + \eta|y'| \tag{24}$$

The shapes for components utilizing different values for η are presented in Figs. 12(b) and 12(c). Using new components with this extra design variable (8 design variables per component), the optimum topology for a cantilever beam (Fig. 13(a)) with a 50% mass constraint was obtained. The optimum layouts using both 7 and 8 design variables for each component can be seen in Figs. 13(b) and 13(c), respectively. The start and end points of the bars usually overlapped with each other but new design variables could slightly reduce the compliance. The layout was almost the same in both Figs. 13(b) and 13(c). The extra design variable obviously led to an increase in computational costs.

3.2. Thermo-mechanical example

In addition to the stress and strain due to mechanical loads, there may be stress and strain within structures due to thermal expansion and contraction. These types of problems with both mechanical and thermal loads are referred to as thermo-mechanical problems. Mathematical formulations of the thermo-mechanical optimization problem were similar to Eq. (8), and the applied force was the sum of the mechanical and thermal loads:

$$\mathbf{KU} = \mathbf{F}_{mechanical} + \mathbf{F}_{thermal} \tag{25}$$

The thermal load ($\mathbf{F}_{thermal}$) is a design dependent load; therefore, values of the load vector changed during the optimization process:

$$\mathbf{F}_{thermal} = \sum \mathbf{F}^e_{thermal} \quad , \quad \mathbf{F}^e{}_{thermal} = \int_{\Omega_e} \mathbf{B}^T\mathbf{D}\boldsymbol{\varphi}^T\alpha_t\tau d\Omega_e \tag{26}$$

Here, changes in temperature and thermal expansion coefficient are denoted by $\tau = \tau(\mathbf{x})$ and α_t, respectively. Moreover, $\mathbf{D}$ represents material tensor, $\mathbf{B}$ stands for gradient matrix and for 2D, $\boldsymbol{\varphi}$ is the following vector:

$$\boldsymbol{\varphi} = [1 \quad 1 \quad 0] \tag{27}$$

By calculating the shape derivative of a very small hole in a thermo-elastic structure, the following topological derivative can be obtained [66]:

$$T = \frac{4}{1+\nu}\boldsymbol{\sigma}(\mathbf{u}): \boldsymbol{\varepsilon}(\mathbf{u}) - \frac{1-3\nu}{1-\nu^2}\mathrm{tr}\boldsymbol{\sigma}(\mathbf{u})\mathrm{tr}\boldsymbol{\varepsilon}(\mathbf{u}) - \frac{2\alpha_t\tau}{1-\nu}\mathrm{tr}\boldsymbol{\sigma}(\mathbf{u}) - \frac{2E\alpha_t^2\tau^2}{1-\nu} \tag{28}$$

The difference between Eqs. (16) and (28) can be seen in the

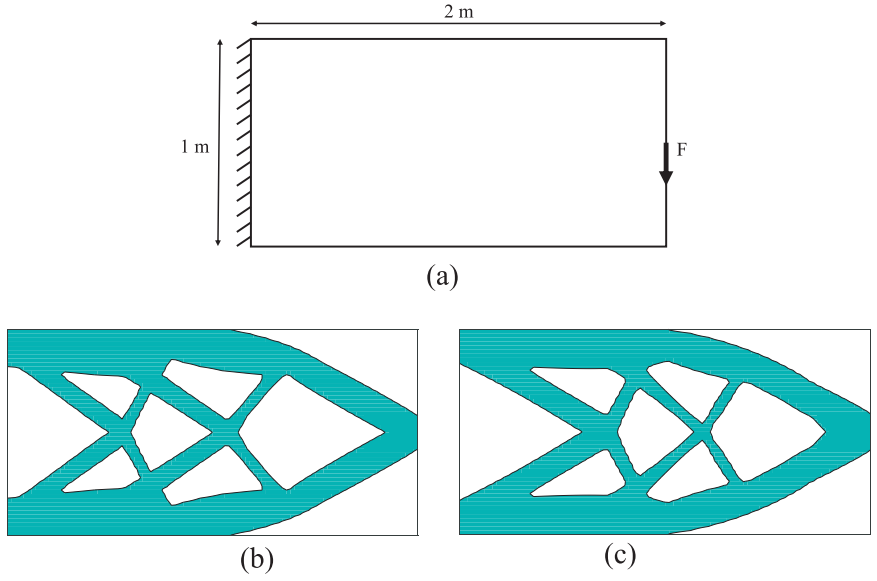

Fig. 13. The cantilever beam; (a) its initial domain and optimum layout with (b) 7 design variables ($C = 60.687$ J) and (c) 8 design variables ($C = 60.473$ J).

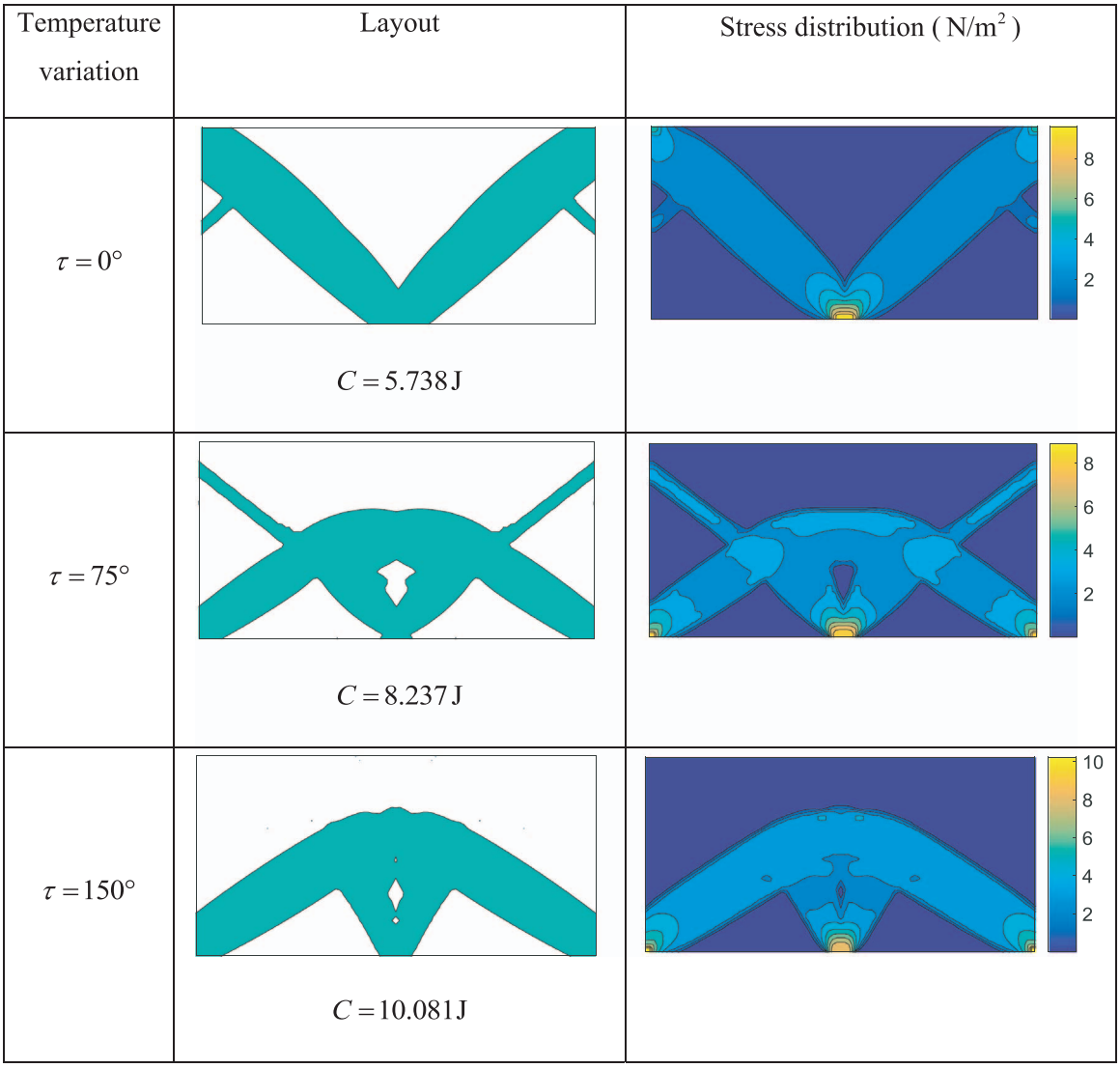

Fig. 14. Optimization results with some different temperature distributions (temperature in degrees centigrade).

following extra terms: $-\frac{2\alpha_t \tau}{1-\nu}\mathrm{tr}\boldsymbol{\sigma}(\mathbf{u}) - \frac{2E\alpha_t^2\tau^2}{1-\nu}$. Here, the stress field should be calculated under both mechanical loadings and temperature changes:

$$\boldsymbol{\sigma}(\mathbf{u}) = \mathbf{C}\boldsymbol{\varepsilon}(\mathbf{u}) - \frac{E\alpha_t \tau}{1-\nu}\mathbf{I} \tag{29}$$

where $\mathbf{I}$ is the identity matrix. The optimum layouts for the problem previously introduced in Fig. 8 were obtained under different uniform temperature changes. Again, the mass limit was set to 40%. The optimum topologies and von Mises stress distributions can be seen in Fig. 14. By increasing the temperature, the optimal layout was changed from two bars with tension loads (near downward arc) to an upward arc and the apex of the arch shape design under the present boundary conditions moved in a direction opposite to that of the curvature due to thermal strain. On the other hand, displacement of the apex under an applied mechanical load was in the direction of the load. Hence, if these two movements were in opposite directions, then the total strain energy would be less. This explained the change in the optimal layout during an elevation in temperature.

3.3. Stress minimization examples

Although compliance minimization is more popular in TO due to its simplicity, stress based TO is more practical with regard to engineering although more difficult in implementation [10,24]. Stress-based TO problems considered stress as an objective function or a constraint, which could be written in a mathematical form using the MMC approach as follows:

$$\begin{aligned} &\text{Find } \mathbf{DV} = \{\mathbf{DV}_1, \mathbf{DV}_2, \ldots, \mathbf{DV}_i, \ldots, \mathbf{DV}_N\} \\ &\underset{\Omega \subset D}{\text{Min}} \quad \text{Maximum stress} = \sigma_{\max} \\ &\text{Subject to:} \\ &\qquad |\Omega| = |\Omega|^* \\ &\qquad \mathbf{KU} = \mathbf{F} \end{aligned} \tag{30}$$

This optimization formulation was intended to minimize the maximum stress inside the design domain. The topological derivative at any point of the domain for the formulation of this stress constrained TO problem could be obtained from the following equation [22]:

$$T = \frac{4}{1+\nu}\boldsymbol{\sigma}(\mathbf{u}) : \boldsymbol{\varepsilon}(\boldsymbol{\lambda}) - \frac{1-3\nu}{1-\nu^2}\mathrm{tr}\boldsymbol{\sigma}(\mathbf{u})\mathrm{tr}\boldsymbol{\varepsilon}(\boldsymbol{\lambda}) \tag{31}$$

Here, $\boldsymbol{\varepsilon}(\boldsymbol{\lambda})$ is the strain tensor computed from the adjoint field, calculated by [42]:

$$\mathbf{K}\boldsymbol{\lambda} = -\nabla_{\mathbf{U}}\psi \tag{32}$$

The maximum stress inside the design domain was approximated by the p-norm approach as follows [30]:

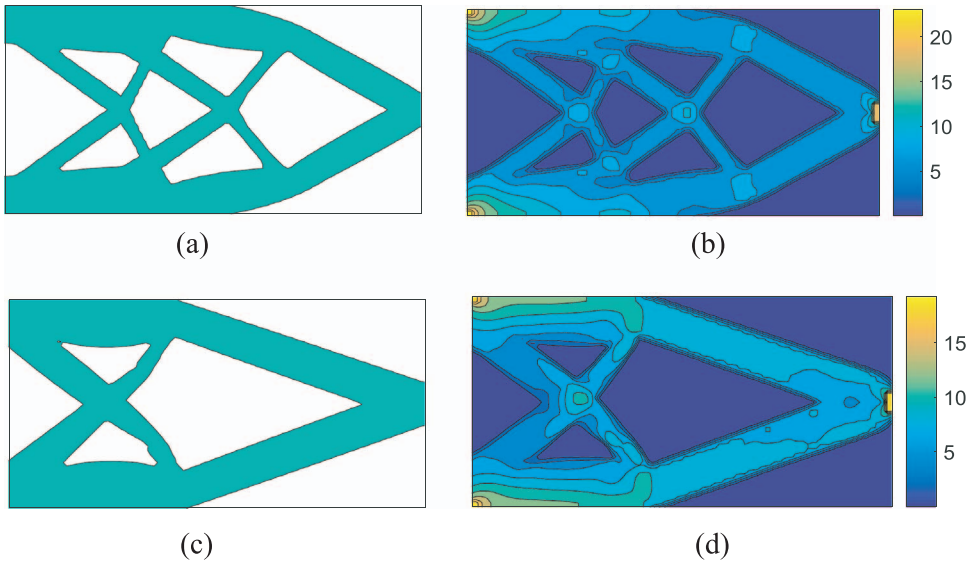

Fig. 15. Optimum layout for the cantilever beam problem ($|\Omega|^* = 0.5\,|\Omega|_{initial}$). (a) Compliance minimization ($C = 60.687$ J, $\sigma_{max} = 23.031\ N/m^2$) and (b) stress minimization ($C = 67.001$ J, $\sigma_{max} = 19.245\ N/m^2$).

$$\sigma_{max} \cong \psi = \left(\sum (\sigma^e)^p \right)^{\frac{1}{p}} \tag{33}$$

Higher values for p will lead to better approximations, but may create numerical instabilities [22]. As the p-norm is used for the objective function (not for the constraint), a correction factor is not necessary. In Eq. (33), σ^e is the stress calculated at the center of the element. If one chooses the von Mises criteria, σ^e can be expressed via stress tensor components as follows:

$$\sigma^e = \left(\frac{1}{\sqrt{2}}\right)\left(\sqrt{(\sigma_{11}-\sigma_{22})^2 + (\sigma_{22}-\sigma_{33})^2 + (\sigma_{33}-\sigma_{11})^2 + 6\sigma_{12}\sigma_{12} + 6\sigma_{13}\sigma_{13} + 6\sigma_{23}\sigma_{23}}\right) \tag{34}$$

Therefore, the desired sensitivity of ψ with respect to a nodal displacement $\mathbf{U}$ (required in Eq. (32)) can be computed as follows:

$$-\nabla_{\mathbf{U}}\psi = -\frac{\partial \psi}{\partial \mathbf{U}} = -\frac{1}{p}\left(\sum (\sigma^e)^p \right)^{\frac{1}{p}-1} \left[\sum p\,(\sigma^e)^{p-1} \frac{\partial \sigma^e}{\partial \mathbf{U}} \right] \tag{35}$$

where:

$$\frac{\partial \sigma^e}{\partial \mathbf{U}} = \left(\frac{1}{2\sigma^e}\right) \times$$

$$\begin{pmatrix} (\sigma_{11}-\sigma_{22})((\mathbf{DB})_{1,:} - (\mathbf{DB})_{2,:}) + (\sigma_{22}-\sigma_{33})((\mathbf{DB})_{2,:} - (\mathbf{DB})_{3,:}) \\ +(\sigma_{33}-\sigma_{11})((\mathbf{DB})_{3,:} - (\mathbf{DB})_{1,:}) \\ +6\sigma_{12}(\mathbf{DB})_{4,:} + 6\sigma_{13}(\mathbf{DB})_{5,:} + 6\sigma_{23}(\mathbf{DB})_{6,:} \end{pmatrix} \tag{36}$$

By substituting Eq. (36) into Eq. (35), the right side of Eq. (32) will be obtained. Once the adjoint field from solving the linear equation system (Eq. (32)) was computed, the stress topological sensitivity field could be calculated from Eq. (31).

3.3.1. Example 1: Compliance and stress minimization of a cantilever beam problem

The simple cantilever beam problem (Fig. 13(a)) was solved for both the compliance and stress minimization formulations (Eq. (8) and Eq. (30)). The mass limit was set to 50% of the initial mass and the value p in the p-norm formula (Eq. (33)) was selected to be 10. The same as the clamped beam example, 5000 elements with 16 components were used for FE analysis and TO. The optimum layout for compliance and stress minimization can be seen in Fig. 15(a) and (c), respectively. Moreover, the von Mises stress distributions for these layouts are depicted in Fig. 15(b) and (d). As expected, for the same volume, the maximum stress in the layout obtained from the stress minimization formula (Fig. 15(d)) was less than this value, which was obtained by compliance minimization formulation (Fig. 15(b)). Additionally, compliance increased in the layout shown in Fig. 15(c) compared to the layout represented in Fig. 15(a).

3.3.2. Example 2: L-bracket example

The next example, which was solved by the stress minimization formula, is an L-bracket example which a unit load was applied at the top right (Fig. 16(a)). The final mass was set to 50% of the initial value and the number of design variables were 224. The optimum layout in the compliance minimization approach had a stress concentration point at the corner of the bracket. If this problem was solved by the MMC approach using the compliance minimization formulation, the same layout would be obtained (Figs. 16(b) and (c)). By utilizing the topological derivative for the stress minimization problem in the MMC approach, the desired optimum layout was achieved (Fig. 16(d)). The von Mises stress distribution for this layout can be seen in Fig. 16(e). Here, the 90° corner vanished and the maximum stress was less than this value compared to the optimal compliance minimization layout.

4. Conclusions

This study developed an MMC framework approach based on continuum structural sensitivity analysis. The first derivative of the compliance with respect to the component shape and position values was calculated by the concept of the topological derivative. The obtained formula was validated via discrete sensitivity analysis, which was calculated based on the finite element method. The developed sensitivity was utilized in the MMC framework approach to solve several types of structural TO problems such as thermo-mechanical and stress-based TO. The provided examples demonstrated the capability and efficiency of the developed MMC framework approach. This approach could be used to solve other types of TO problems with known topological derivative.

Acknowledgements

This work was supported by the research fund of Hanyang University (HY-2017) and the National Research Foundation of Korea (NRF) grant funded by the Korea government (MEST) (NRF-2015R1A2A2A11027580).

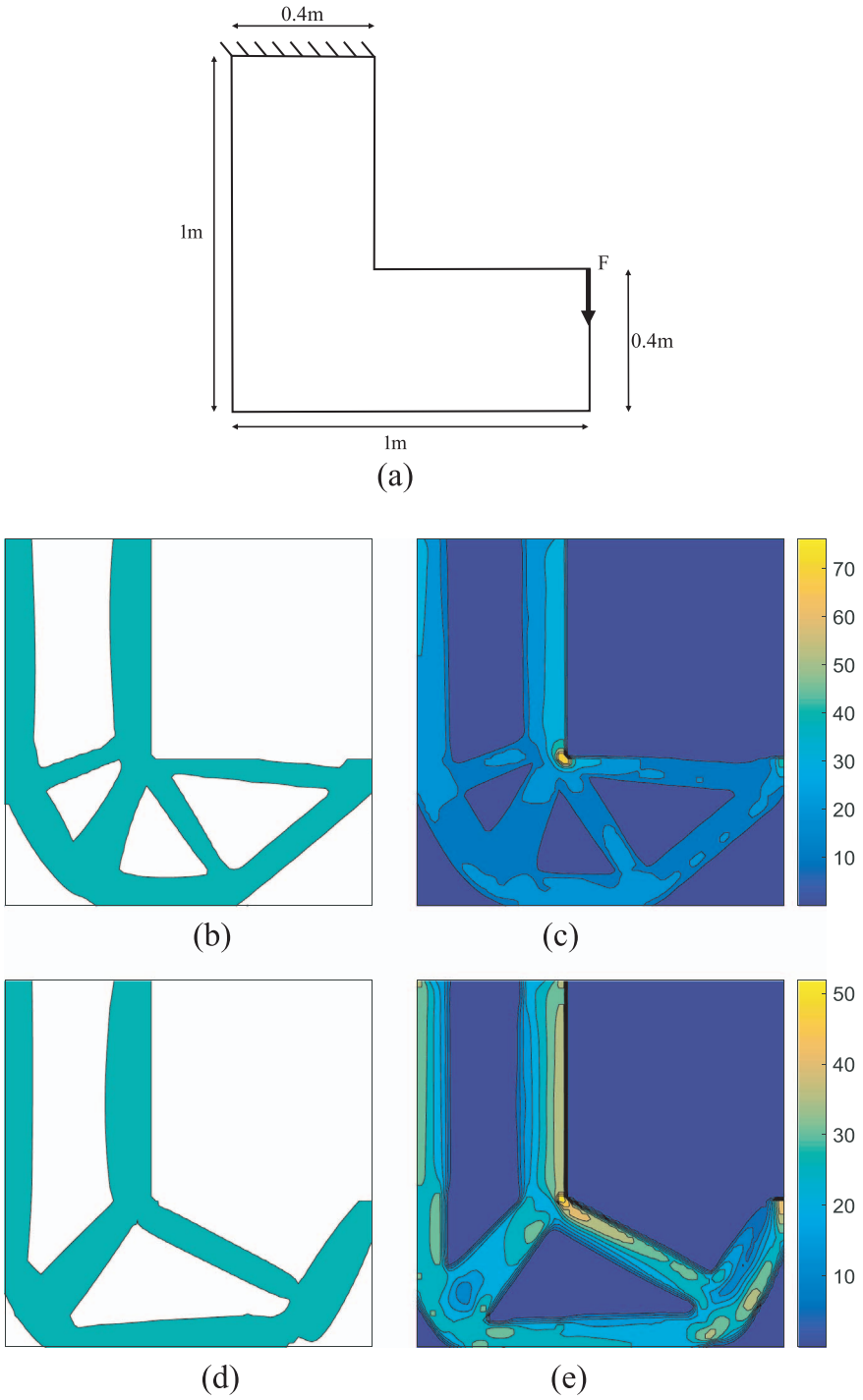

Fig. 16. The L-bracket; (a) its initial domain and optimal layout, (b), (c) compliance minimization layout and stress distribution ($C = 165.295$ J, $\sigma_{max} = 76.192\ N/m^2$), and (d), (e) the stress minimization layout and stress distribution ($C = 208.742$ J, $\sigma_{max} = 51.846\ N/m^2$).

References

[1] G.I.N. Rozvany, A critical review of established methods of structural topology optimization, Struct. Multidiscip. Optim. 37 (2009) 217–237.

[2] M.P. Bendsøe, N. Kikuchi, Generating optimal topologies in structural design using a homogenization method, Comput. Methods Appl. Mech. Eng. 71 (1988) 197–224.

[3] M.P. Bendsøe, Optimal shape design as a material distribution problem, Struct. Optim. 1 (1989) 193–202.

[4] S.J. Osher, F. Santosa, Level set methods for optimization problems involving geometry and constraints: i. Frequencies of a two-density inhomogeneous drum, J. Comput. Phys. 171 (2001) 272–288.

[5] G. Allaire, F. Jouve, A.-M. Toader, A level-set method for shape optimization, Comptes Rendus Math. 334 (2002) 1125–1130.

[6] G. Allaire, F. Jouve, A.-M. Toader, Structural optimization using sensitivity analysis and a level-set method, J. Comput. Phys. 194 (2004) 363–393.

[7] Y.X. Du, Z. Luo, Q.H. Tian, L.P. Chen, Topology optimization for thermo-mechanical compliant actuators using mesh-free methods, Eng. Optim. 41 (2009) 753–772.

[8] X. Guo, W.S. Zhang, W.L. Zhong, Doing topology optimization explicitly and geometrically-a new moving morphable components based framework, J Appl. Mech.-Trans. Asme 81 (2014).

[9] G.H. Yoon, Y.Y. Kim, The role of S-shape mapping functions in the SIMP approach for topology optimization, KSME Int. J. 17 (2003) 1496–1506.

[10] P. Duysinx, L. Van Miegroet, E. Lemaire, O. Brüls, M. Bruyneel, Topology and generalized shape optimization: why stress constraints are so important?, Int. J. Simul. Multidiscip. Des. Optim. 2 (2008) 253–258.

[11] O. Sigmund, A 99 line topology optimization code written in Matlab, Struct. Multidiscip. Optim. 21 (2001) 120–127.

[12] G.H. Yoon, Topological layout design of electro-fluid-thermal-compliant actuator, Comput. Methods Appl. Mech. Eng. 209 (2012) 28–44.
[13] G.H. Yoon, Y.Y. Kim, The element connectivity parameterization formulation for the topology design optimization of multiphysics systems, Int. J. Numer. Methods Eng. 64 (2005) 1649–1677.
[14] Z.Y. Liu, J.G. Korvink, M.L. Reed, Multiphysics for structural topology optimization, Sens. Lett. 4 (2006) 191–199.
[15] A. Takezawa, G.H. Yoon, S.H. Jeong, M. Kobashi, M. Kitamura, Structural topology optimization with strength and heat conduction constraints, Comput. Methods Appl. Mech. Eng. 276 (2014) 341–361.
[16] K.-S. Yun, S.-K. Youn, Multi-material topology optimization of viscoelastically damped structures under time-dependent loading, Finite Elem. Anal. Des. 123 (2017) 9–18.
[17] M.Y. Wang, X. Wang, D. Guo, A level set method for structural topology optimization, Comput. Methods Appl. Mech. Eng. 192 (2003) 227–246.
[18] D. Guirguis, M.F. Aly, A derivative-free level-set method for topology optimization, Finite Elem. Anal. Des. 120 (2016) 41–56.
[19] S.G. Deng, K. Suresh, Multi-constrained topology optimization via the topological sensitivity, Struct. Multidiscip. Optim. 51 (2015) 987–1001.
[20] N.P. van Dijk, K. Maute, M. Langelaar, F. van Keulen, Level-set methods for structural topology optimization: a review, Struct. Multidiscip. Optim. 48 (2013) 437–472.
[21] X. Guo, W.S. Zhang, M.Y. Wang, P. Wei, Stress-related topology optimization via level set approach, Comput. Methods Appl. Mech. Eng. 200 (2011) 3439–3452.
[22] K. Suresh, M. Takalloozadeh, Stress-constrained topology optimization: a topological level-set approach, Struct. Multidiscip. Optim. 48 (2013) 295–309.
[23] W.S. Zhang, X. Guo, M.Y. Wang, P. Wei, Optimal topology design of continuum structures with stress concentration alleviation via level set method, Int. J. Numer. Methods Eng. 93 (2013) 942–959.
[24] R.J. Yang, C.J. Chen, Stress-based topology optimization, Struct. Optim. 12 (1996) 98–105.
[25] S.H. Jeong, S.H. Park, D.H. Choi, G.H. Yoon, Toward a stress-based topology optimization procedure with indirect calculation of internal finite element information, Comput. Math. Appl. 66 (2013) 1065–1081.
[26] G.D. Cheng, X. Guo, epsilon-relaxed approach in structural topology optimization, Struct. Optim. 13 (1997) 258–266.
[27] M. Bruggi, On an alternative approach to stress constraints relaxation in topology optimization, Struct. Multidiscip. Optim. 36 (2008) 125–141.
[28] M. Stolpe, K. Svanberg, On the trajectories of the epsilon-relaxation approach for stress-constrained truss topology optimization, Struct. Multidiscip. Optim. 21 (2001) 140–151.
[29] J. Paris, F. Navarrina, I. Colominas, M. Casteleiro, Topology optimization of continuum structures with local and global stress constraints, Struct. Multidiscip. Optim. 39 (2009) 419–437.
[30] C. Le, J. Norato, T. Bruns, C. Ha, D. Tortorelli, Stress-based topology optimization for continua, Struct. Multidiscip. Optim. 41 (2010) 605–620.
[31] H. Rodrigues, P. Fernandes, A material based model for topology optimization of thermoelastic structures, Int. J. Numer. Methods Eng. 38 (1995) 1951–1965.
[32] Q. Xia, M.Y. Wang, Topology optimization of thermoelastic structures using level set method, Comput. Mech. 42 (2008) 837–857.
[33] J.D. Deaton, R.V. Grandhi, Stiffening of restrained thermal structures via topology optimization, Struct. Multidiscip. Optim. 48 (2013) 731–745.
[34] W.M. Rubio, S. Nishiwaki, E.C.N. Silva, Design of compliant mechanisms considering thermal effect compensation and topology optimization, Finite Elem. Anal. Des. 46 (2010) 1049–1060.
[35] S. Chen, M.Y. Wang, A.Q. Liu, Shape feature control in structural topology optimization, Comput. Aided Des. 40 (2008) 951–962.
[36] J. Guest, Imposing maximum length scale in topology optimization, Struct. Multidiscip. Optim. 37 (2009) 463–473.
[37] O. Sigmund, Manufacturing tolerant topology optimization, Acta Mech. Sin. 25 (2009) 227–239.
[38] X. Guo, W.S. Zhang, W.L. Zhong, Explicit feature control in structural topology optimization via level set method, Comput. Methods Appl. Mech. Eng. 272 (2014) 354–378.
[39] W.S. Zhang, W.L. Zhong, X. Guo, An explicit length scale control approach in SIMP-based topology optimization, Comput. Methods Appl. Mech. Eng. 282 (2014) 71–86.
[40] W. Zhang, J. Yuan, J. Zhang, X. Guo, A new topology optimization approach based on Moving Morphable Components (MMC) and the ersatz material model, Struct. Multidiscip. Optim. 53 (2016) 1243–1260.
[41] W. Zhang, D. Li, J. Yuan, J. Song, X. Guo, A new three-dimensional topology optimization method based on moving morphable components (MMCs), Comput. Mech. (2016) 1–19.
[42] K.K. Choi, N.-H. Kim, Structural Sensitivity Analysis and Optimization 1: Linear Systems, Springer Science & Business Media, New York, US, 2006.
[43] H.A. Eschenauer, V.V. Kobelev, A. Schumacher, Bubble method for topology and shape optimization of structures, Struct. Optim. 8 (1994) 42–51.
[44] A. Novotny, R. Feijóo, E. Taroco, C. Padra, Topological sensitivity analysis for three-dimensional linear elasticity problem, Comput. Methods Appl. Mech. Eng. 196 (2007) 4354–4364.
[45] I. Turevsky, S.H. Gopalakrishnan, K. Suresh, An efficient numerical method for computing the topological sensitivity of arbitrary-shaped features in plate bending, Int. J. Numer. Methods Eng. 79 (2009) 1683–1702.
[46] A.A. Novotny, J. Sokołowski, Topological Derivatives in Shape Optimization, Springer Science & Business Media, Berlin, Heidelberg, 2012.
[47] J. Sokolowski, A. Zochowski, On the topological derivative in shape optimization, SIAM J. Control Optim. 37 (1999) 1251–1272.
[48] A.A. Novotny, R.A. Feijóo, E. Taroco, C. Padra, Topological sensitivity analysis, Comput. Methods Appl. Mech. Eng. 192 (2003) 803–829.
[49] K. Suresh, A 199-line Matlab code for Pareto-optimal tracing in topology optimization, Struct. Multidiscip. Optim. 42 (2010) 665–679.
[50] S. Deng, K. Suresh, Multi-constrained 3D topology optimization via augmented topological level-set, Comput. Struct. 170 (2016) 1–12.
[51] S. Amstutz, A.A. Novotny, Topological optimization of structures subject to von Mises stress constraints, Struct. Multidiscip. Optim. 41 (2010) 407–420.
[52] S. Amstutz, A.A. Novotny, E.A.D. Neto, Topological derivative-based topology optimization of structures subject to Drucker-Prager stress constraints, Comput. Methods Appl. Mech. Eng. 233 (2012) 123–136.
[53] A. Krishnakumar, K. Suresh, Hinge-free compliant mechanism design via the topological level-set, J. Mech. Des. 137 (2015) 031406.
[54] C.G. Lopes, A.A. Novotny, Topology design of compliant mechanisms with stress constraints based on the topological derivative concept, Struct. Multidiscip. Optim. 54 (2016) 737–746.
[55] S. Giusti, A. Novotny, J. Sokołowski, Topological derivative for steady-state orthotropic heat diffusion problem, Struct. Multidiscip. Optim. 40 (2010) 53.
[56] C.G. Lopes, Santos RBd, A.A. Novotny, Topological derivative-based topology optimization of structures subject to multiple load-cases, Lat. Am. J Solids Struct. 12 (2015) 834–860.
[57] A.A.S. Amad, A.F.D. Loula, A.A. Novotny, A new method for topology design of electromagnetic antennas in hyperthermia therapy, Appl. Math. Model. 42 (2017) 209–222.
[58] A. Canelas, A.A. Novotny, J.R. Roche, A new method for inverse electromagnetic casting problems based on the topological derivative, J. Comput. Phys. 230 (2011) 3570–3588.
[59] S.M. Giusti, A.A. Novotny, J.E.M. Rivera, J.E.E. Rodriguez, Strain energy change to the insertion of inclusions associated to a thermo-mechanical semi-coupled system, Int. J. Solids Struct. 50 (2013) 1303–1313.
[60] M. Takalloozadeh, G.H. Yoon, Development of Pareto topology optimization considering thermal loads, Comput. Methods Appl. Mech. Eng. 317 (2017) 554–579.
[61] N. Van Goethem, A.A. Novotny, Crack nucleation sensitivity analysis, Math. Method Appl. Sci. 33 (2010) 1978–1994.
[62] A. Khludnev, J. Sokolowski, K. Szulc, Shape and topological sensitivity analysis in domains with cracks, Appl. Math. 55 (2010) 433–469.
[63] L.F.N. Sa, R.C.R. Amigo, A.A. Novotny, E.C.N. Silva, Topological derivatives applied to fluid flow channel design optimization problems, Struct. Multidiscip. Optim. 54 (2016) 249–264.
[64] K. Abe, T. Fujiu, K. Koro, A BE-based shape optimization method enhanced by topological derivative for sound scattering problems, Eng. Anal. Bound. Elem. 34 (2010) 1082–1091.
[65] R. Feijoo, A. Novotny, E. Taroco, C. Padra, The topological-shape sensitivity method in two-dimensional linear elasticity topology design, Appl. Comput. Mech. Struct. Fluids (2005).
[66] M. Takalloozadeh, G.H. Yoon, Development of Pareto topology optimization considering thermal loads, Comput. Methods Appl. Mech. Eng. 317 (2017) 554–579.